RSC Advances

PAPER

View Article Online
View Journal | View Issue

Published on 11 August 2016. Downloaded by Synchrotron Radiation Library on 11/09/2017 09:57:49.

Cite this: *RSC Adv.*, 2016, **6**, 78008

Highly coplanar bis(thiazol-2-yl)-diketopyrrolopyrrole based donor–acceptor copolymers for ambipolar field effect transistors†

Dong Gao,‡[ab] Zhihui Chen,‡[ab] Zupan Mao,[a] Jianyao Huang,[a] Weifeng Zhang,[a] Dizao Li[a] and Gui Yu*[ab]

Received 5th July 2016
Accepted 11th August 2016

DOI: 10.1039/c6ra17241e

www.rsc.org/advances

The coplanarity and intermolecular interactions of polymers are fundamental factors influencing intra- or interchain charge transport for polymer field-effect transistors (PFETs). In this work, four alternating donor–acceptor copolymers with the acceptor of bis(thiazol-2-yl)-diketopyrrolopyrrole (TZDPP) and donor of (*E*)-1,2-di(thiophen-2-yl)ethene (TVT) or (*E*)-1,2-di(selenophen-2-yl)ethene (SVS) were synthesized. The introduction of thiazole units promotes the coplanarity of the polymer backbone. In addition, the electron deficient properties of TZDPP enhance interchain interactions. The polymers exhibited ambipolar semiconducting behaviours with the highest hole and electron mobilities reaching 0.17 and 9.7 $\times$ 10^{-3} cm^2 V^{-1} s^{-1}, respectively, in top-gate bottom-contact PFET devices. The SVS-based polymers showed lower mobilities than those containing TVT units. Careful characterization of the polymer films revealed that though the polymers containing SVS units exhibited better crystallinity, their films were less ordered and less uniform, which may arise from the limited solubility of the polymers. These results suggest the critical role of solubility in the fabrication of devices, and the interchain interactions should be controlled in an appropriate manner.

Introduction

Over the past decades, π-conjugated polymer semiconductors for organic field-effect transistors (OFETs) have been attracting considerable attention due to their easily modified structure, solution processability, superior mechanical properties, and inexpensive device fabrication.[1] The optimization of the molecular structure is one of top issues to achieve high OFET device performance. Great achievements in polymer field-effect transistors (PFETs) have been obtained through molecular design. Among all the molecule design methods, the so called "donor–acceptor (D–A)" design strategy has been utilized in synthesizing high-performance conjugated polymers for PFETs and some D–A copolymers exhibited high hole or electron mobilities exceeding 1.0 cm^2 V^{-1} s^{-1}, which could compete with the performance of amorphous silicon.[2]

In the design strategy of D–A copolymers, an electron density gradient along the polymer backbone is created by introducing "electron rich" and "electron-deficient" segments to the backbone, thus offering a lower energy charge-transfer transition. The energy levels and band gaps of the polymers can be easily adjusted by using different donor or acceptor in the backbone of polymer *via* the intramolecular charge transfer (ICT). In addition to intrinsic optoelectronic properties of the polymers, self-assembly processes are also affected by the noncovalent interchain interactions induced by the D–A structures. Conjugated polymers with alternating D–A structures demonstrate close π–π stacking distances, which are beneficial for approaching high mobilities.[3] For the building blocks of D–A copolymers, the acceptor moieties play a much more important role in determining the electronic behaviour and intermolecular interaction of the polymers. Hole transport behaviour has been observed in most D–A polymers, while the electron transport is dependent on the type of acceptor.[4] Energy level of the lowest unoccupied molecular orbital (LUMO) for the resulting polymer is mainly affected by the electron poor component of accepter.[5] A stronger accepting moieties with low-lying LUMO energy levels can significantly lower the LUMO ones of corresponding polymers, which are essential for obtaining n-type or ambipolar semiconductors. Theoretical calculation and experimental results also revealed that introducing high electronegativity atoms to acceptor moieties could enhance the strength of non-covalent interactions among polymer chains, thus offering stronger π–π interactions and tendency to aggregate, which, in turn, enable higher performance for transistors.[5c]

[a]*Beijing National Laboratory for Molecular Sciences, Institute of Chemistry, Chinese Academy of Sciences, Beijing 100190, P. R. China. E-mail: yugui@iccas.ac.cn*

[b]*University of Chinese Academy of Sciences, Beijing 100049, P. R. China*

† Electronic supplementary information (ESI) available. See DOI: 10.1039/c6ra17241e

‡ These authors contributed equally to this work.

This journal is © The Royal Society of Chemistry 2016

Published on 11 August 2016. Downloaded by Synchrotron Radiation Library on 11/09/2017 09:57:49.

Herein, we synthesized four bis(thiazol-2-yl)-diketopyrrolopyrrole (TZDPP)-based D–A copolymers with the (*E*)-1,2-di(thiophen-2-yl)ethene (TVT) or (*E*)-1,2-di(selenophen-2-yl) ethene (SVS) as corresponding donor moieties. With the strong electron deficient properties of thiazole and diketopyrrolopyrrole, TZDPP acts as a strong acceptor in D–A copolymers, and the TZDPP-based polymers have been employed as an electron acceptor in all-polymer solar cells and as an active layer in ambipolar OFETs.[6] TVT- and SVS-containing D–A copolymers have been reported to exhibit excellent p- or n-type charge carrier transporting properties due to the extended coplanarity and promoted intermolecular π–π stacking.[2a,c,7] Theoretical results suggested that the TZDPP units exhibit quite good coplanarity. By introducing the strong acceptor of TZDPP to the TVT- or SVS-containing polymers, a low-lying LUMO energy levels were achieved, which are beneficial for electron injection from Au electrode. The characterization of the thin films also revealed strong interchain interaction among polymer chains, especially for the SVS-based copolymers. To investigate the ambipolar behaviour of the semiconductors, top-gate bottom-contact (TGBC) FETs were fabricated and exhibited ambipolar charge carrier transport properties with hole and electron mobilities reaching 0.17 and 9.7 × 10^{-3} cm^2 V^{-1} s^{-1}, respectively.

Experimental

Materials and characterization techniques

All the chemical regents were purchased without further purification. Solvents were purified and dried by following standard procedures if necessary. Compounds 1 and 2 (Scheme 1) were synthesized according to reported procedures.[2a,c,6,7]

^{1}H NMR spectra were recorded on Bruker Avance 300 MHz spectrometer at 100 °C. Gel-permeation chromatography (GPC) was performed on a Agilent PL-GPC 220 with polystyrene as a standard and 1,2,4-trichlorobenzene as an eluent. UV-vis absorption spectra were measured in solutions and drop-coasted thin films using a J-570 spectrometer. Cyclic voltammetry (CV) experiments were conducted on an electrochemistry workstation (CHI660c, Chenhua Shanghai) with a three-electrode cell. Ag/AgCl (Ag in a 0.01 mol L^{-1} KCl) electrode was used as a reference electrode and platinum wire was employed as a counter electrode. Platinum stick electrode coated with a thin film layer of polymer was used as a working electrode. An anhydrous and N_2-saturated solution of 0.1 M tetrabutylammonium hexylfluorophosphate in acetonitrile was employed as an electrolyte. The HOMO and LUMO energy levels were estimated with the onset of the corresponding oxidative peaks and reductive peaks of the polymers using the equations $E_{HOMO} = -(E_{ox}^{onset} + 4.4)$ eV and $E_{LUMO} = -(E_{re}^{onset} + 4.4)$ eV. Thermogravimetric analysis (TGA) was performed on a Perkin-Elmer TGA-7 with a heating rate of 10 °C min^{-1} under nitrogen atmosphere. The films of the polymers were imaged in air using a Digital Instruments Nanoscope V atomic force microscope operated in a tapping mode, which were identical to those characterized in the respective PFETs.

Synthesis of PTD-8-TVT, PTD-10-TVT, PTD-8-SVS and PTD-10-SVS

In a Schlenk flask, monomer 1 (0.2 mmol), TZDPP monomer 2 (0.2 mmol), tris(dibenzylideneacetone)dipalladium (0) (4.5 mg), and tri(*o*-tolyl)phosphine (12.3 mg) were dissolved in dry toluene (5 mL). The solution was charged with nitrogen through a freeze–pump–thaw cycle for three times. Then mixture was stirred at 110 °C for 2 h under nitrogen atmosphere. The polymer was precipitated in methanol after cooling down to room temperature. The crude polymer was collected by filtration and then purified by Soxhlet extraction with methanol, acetone, hexane, chloroform to remove low molecular weight component and chlorobenzene was finally used to extract the target product. The evaporation of chlorobenzene fractions afforded a dark solid.

PTD-8-TVT: yield: 90.3 mg, 43%. ^{1}H NMR (300 MHz, $C_2D_2Cl_4$): $\delta = 7.85$ (br, 6H), 6.96 (br, 2H), 4.29 (br, 4H), 1.68–0.79 (m, 78H).

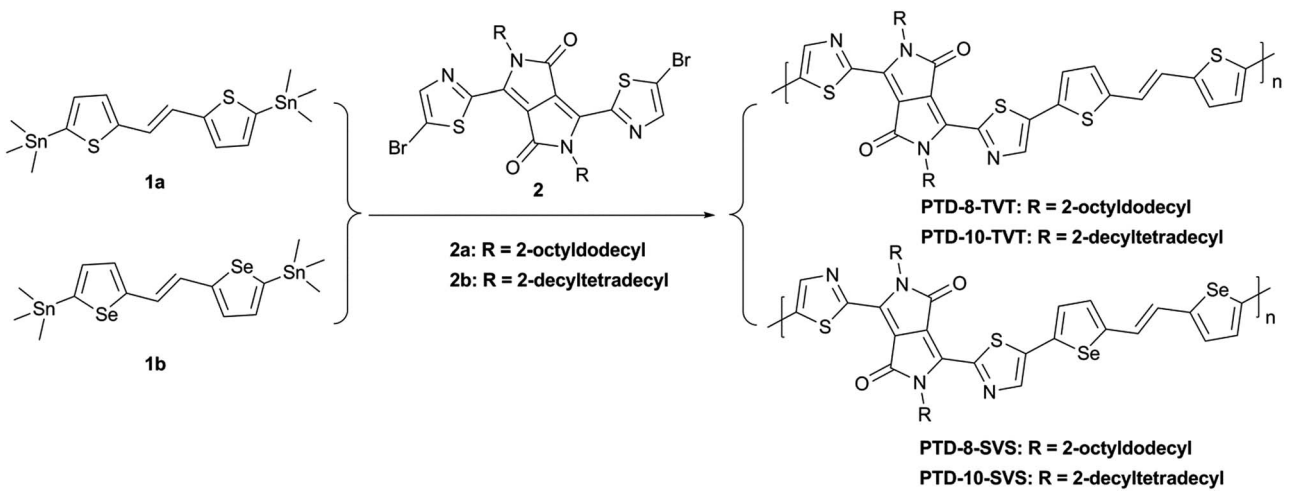

Scheme 1 Synthetic route of TZDPP-based polymers. Regents and conditions: $Pd_2(dba)_3$, P(*o*-tol)$_3$, toluene, 110 °C.

Published on 11 August 2016. Downloaded by Synchrotron Radiation Library on 11/09/2017 09:57:49.

PTD-10-TVT: yield: 118.5 mg, 51%. ^{1}H NMR (300 MHz, $C_2D_2Cl_4$): $\delta = 7.93$ (br, 6H), 6.89 (br, 2H), 4.26 (br, 4H), 1.91–0.80 (m, 94H).

PTD-8-SVS: yield: 169.2 mg, 74%. ^{1}H NMR (300 MHz, $C_2D_2Cl_4$): $\delta = 7.93$ (br, 6H), 6.95 (br, 2H), 4.33 (br, 4H), 1.89–0.80 (m, 78H).

PTD-10-SVS: yield: 118.0 mg, 47%. ^{1}H NMR (300 MHz, $C_2D_2Cl_4$): $\delta = 7.95$ (br, 6H), 6.91 (br, 2H), 4.27 (br, 4H), 1.89–0.80 (m, 94H).

Device fabrication

Top-gate bottom-contact (TGBC) PFET devices were fabricated on silicon dioxide substrates. The substrates were subjected to cleaning with ultrasonication in acetone, deionized water, and ethanol. Then gold source/drain electrodes were formed on the surface of substrates through photolithography (L/W = 50 μm/1400 μm). In a N_2 glovebox, the TZDPP-based polymers dissolved in *o*-DCB (5 mg mL^{-1}) was spin coated onto the silicon substrates, yielding a polymer film with a thickness of ~35 nm. Then polymer films were further annealed for 5 min. Polymethylmethacrylate (PMMA) (M_w = 1000 kDa) solution in anhydrous *n*-butyl acetate (80 mg mL^{-1}) was spin-coated onto the surface of the polymer films. The PMMA thickness is ~1000 nm with capacitance of 2.4 nF cm^{-2}. The samples were then dried at 80 °C for 30 min in vacuum. The aluminum gate electrodes (thickness ~100 nm) were then evaporated through a shadow mask onto the PMMA gate dielectric. These top-gate PFETs were measured in ambient air with relative humidity of 30–60%.

Results and discussion

The synthetic routes of all TZDPP based polymers are shown in Scheme 1. The monomers of TZDPP with different substituent branched side chains and the monomers of TVT and SVS were synthesized according to the previous literature.[2,6,7] Stille copolymerization of tin monomers and TZDPP monomers were conducted to afford the crude copolymers, respectively. After carefully purifying by Soxhlet extraction to remove low-molecular-weight impurities and Pd-based catalyst with methanol, acetone, hexane and chloroform, chlorobenzene was used to extract the target copolymers as black film-like solid in 50–75% yields. The molecular weight (M_n and M_w) and PDI of the copolymers were determined by gel permeation chromatography (GPC) relative to polystyrene standards in hot 1,2,4-trichlorobenzene. All polymers showed relatively high molecule weight, which is essential for achieving high mobilities.[8a,b] However, the broader PDI of the SVS-based polymers indicate the presence of low molecule weight polymers, oligomers and by-products in the polymer mixtures, which may be ascribed to the poor solubility arising from strong intermolecular interactions for selenophen based polymers.[8c,d] The poor solubility may lead to increase in mixture viscosity, thus making the heating and mixing of the mixture uneven. The broad PDI may exert negative effect on the device performance.[8e–g] The polymers are insoluble in chloroform, and show poor solubility in chlorobenzene at room temperature, indicating the strong intermolecular interactions induced by the strong accepter TZDPP. The polymers can be soluble in hot chlorobenzene and dichlorobenzene and highly uniform films can be fabricated with a simple spin-coating technique. Thermal behaviour of the polymers was also measured through TGA under nitrogen atmosphere at a heating rate of 10 °C min^{-1} as shown in Fig. S1.† All polymers have good thermal stability with decomposition temperatures (5% weight loss) of over 300 °C.

To investigate the optical properties of the copolymers, the absorption spectra of the four polymers in the diluted 1,2-dichlorobenzene solution and the thin films were measured.

Typical absorption spectra curves are showed in Fig. 1 and the corresponding parameters are collected in Table 1. All of the polymers exhibit narrow bands at 300–500 nm and broader ones at long wavelength range which can be attributed to the strong ICT between the electron-donating and electron withdrawing units of TZDPP. The ICT absorption bands in thin films show a slight blue shift relative to the corresponding solution spectrum, indicating H-aggregation induced interchain packing in the solid state.[9] Obvious vibronic coupling absorption shoulders at this bands can also be observed and the intensity of these peaks in the film increases compared to those in the respective solution absorption spectra. Compared with the TVT containing polymers, the SVS-based polymers exhibit a red shift of absorption maximum and absorption onset of approximately 25 nm in solution and films, which can be attribute to the greater extent of backbone planarity.[2c] The optical band gaps of the polymers estimated from the absorption onset of the thin films are 1.46, 1.47, 1.41, and 1.42 eV for PTD-8-TVT, PTD-10-TVT, PTD-8-SVS, and PTD-10-SVS, respectively. Molecular orbital energy levels of the polymers were evaluated by performing cyclic voltammetry (CV) (Fig. S2†). All the polymers show similar frontier molecular orbital energy levels with the HOMOs of around −5.4 eV and the LUMOs of around −3.6 eV, indicating the little effect on the energy levels of chalcogen heteroatoms. The low-lying energy levels are attributed to the

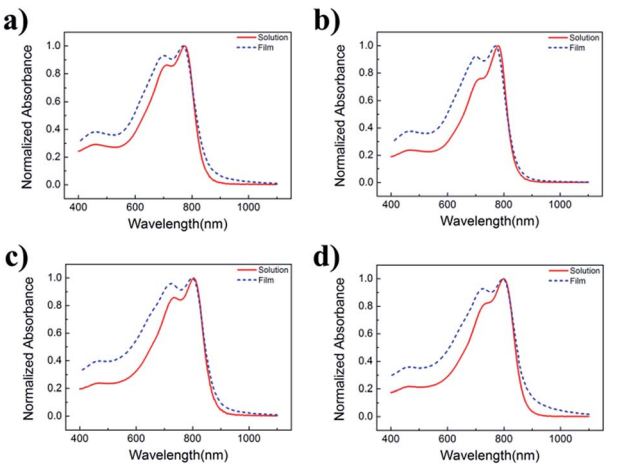

Fig. 1 UV-vis-NIR absorption spectra of (a) PTD-8-TVT, (b) PTD-10-TVT, (c) PTD-8-SVS and (d) PTD-10-SVS in 1,2-dichlorobenzene solution and corresponding thin films.

 This journal is © The Royal Society of Chemistry 2016

Published on 11 August 2016. Downloaded by Synchrotron Radiation Library on 11/09/2017 09:57:49.

Table 1 Properties of TZDPP-based polymers

Polymer	M_n (kDa)	PDI	λ_{max} (solution) (nm)	λ_{max} (film) (nm)	T_d[a] (°C)	E_g (opt)[b] (eV)	E_{HOMO} (eV)	E_{LUMO} (eV)	E_g (ec)[c] (eV)
PTD-8-TVT	19.8	1.71	774	770	331.9	1.46	−5.37	−3.56	1.72
PTD-10-TVT	35.0	2.18	780	770	356.3	1.47	−5.40	−3.64	1.76
PTD-8-SVS	25.1	4.47	804	798	325.5	1.41	−5.38	−3.57	1.81
PTD-10-SVS	61.6	4.07	798	796	326.8	1.42	−5.36	−3.56	1.80

[a] Temperature at 5% weight loss under nitrogen. [b] Estimated from the onset wavelength of the absorption in the films. [c] Estimated from the HOMO and LUMO energy levels.

introduction of strong electron deficient units of TZDPP. The HOMO energy levels of these polymers facilitate the hole injections from the source–drain Au electrodes with a work function of 5.1 eV, to polymeric semiconductors, thus is beneficial to obtaining p-type OFET devices. In addition, relatively low LUMO energy levels of the four polymers are also beneficial for electron injection. The electrochemically bandgaps are slightly higher (0.26–0.4 eV) than optical bandgaps estimated the thin-film absorption onset but can be accepted within the experimental error.

Theoretical calculations were conducted to gain more insight into the optimal conformational structural information. The unit with a thiazole bonded to a diketopyrrolopyrrole with the initial conformation of Fig. 2a was chosen and the torsional potentials between the two units were computed at 10° intervals. In addition, to better understand the conformational preferences of TZDPP in the polymer backbone, a most widely employed acceptor moiety in polymer semiconductors, bis(thiophene-2-yl)-diketopyrrolopyrrole unit (TPDPP), were also calculated.[10] Density functional theory (DFT) has been widely employed in predicting material properties and determining conformational structural because of its accurate ground-state properties and low computational cost. The geometry optimizations were performed at the B3LYP/6-31G(d) level, then these geometries were used as inputs for MP2/cc-pVTZ single-point energy calculations to avoid self-interaction error arising from DFT calculations.[11] The resulting torsional potential energy surfaces are plotted in Fig. 2a. The energy of 180° conformation of TZDPP is lower than that of the initial conformation by 6.74 kcal mol^{-1} with an inversion barrier of 9.04 kcal mol^{-1}, while the 0° conformation of the TPDPP is more stable with the energy difference of 1.79 kcal mol^{-1} and the inversion barrier of 6.71 kcal mol^{-1}. The calculation results show that the 180° conformation is more energetically favourable because of the oxygen–sulphur interaction. Moreover, the larger energy difference and higher inversion barrier of TZDPP compared with those of TPDPP suggest the greater difficulty of conformational change, indicating the better backbone coplanarity and more ordered main chain conformation of the TZDPP-based polymers, which are favour cofacial π–π stacking to improve charge transport.[12] The optimized molecular structures and orbital distributions are plotted in Fig. 2c in which the side chains substituted on diketopyrrolopyrrole moieties were shortened to methyl groups to simplify the calculations. Both polymers exhibit relatively good coplanarity, which is helpful for enhancing intermolecular interactions and improving charge transport. The distributions of frontier orbital for thiophene and selenophene containing polymers show no obvious difference, indicating the negligible effect of the chalcogen heteroatoms. Both the HOMOs and LUMOs of the trimers are delocalized along the polymer backbone, which is beneficial for efficient charge transport.[13]

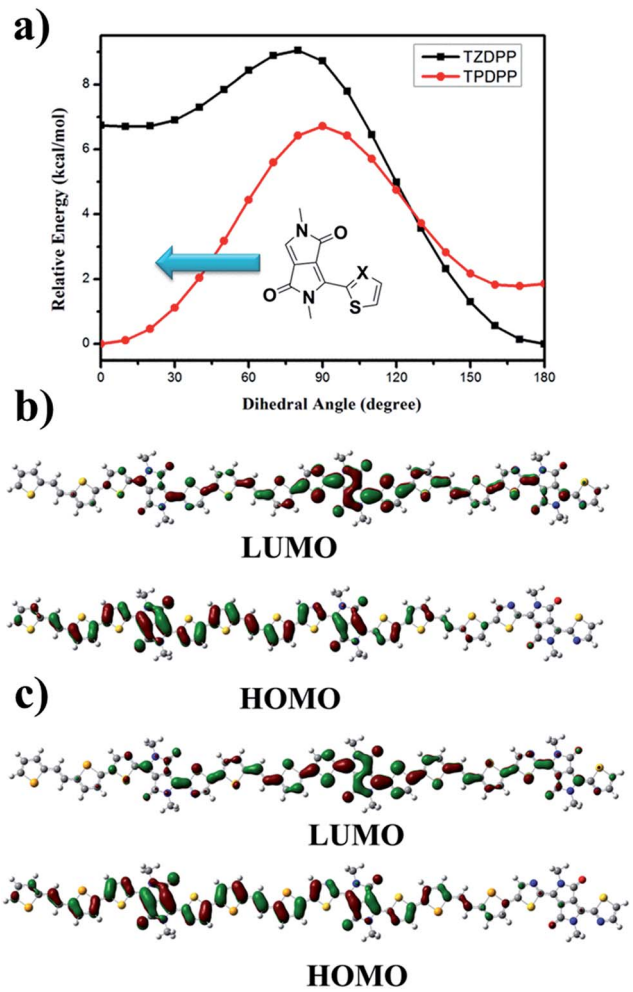

Fig. 2 (a) Theoretical calculation results of torsional potentials for TZDPP (X = N) and TPDPP (X = CH) calculated at the MP2/cc-pVTZ level; the HOMO and LUMO distributions of PTD-TVT (b) and PTD-SVS (c).

Published on 11 August 2016. Downloaded by Synchrotron Radiation Library on 11/09/2017 09:57:49.

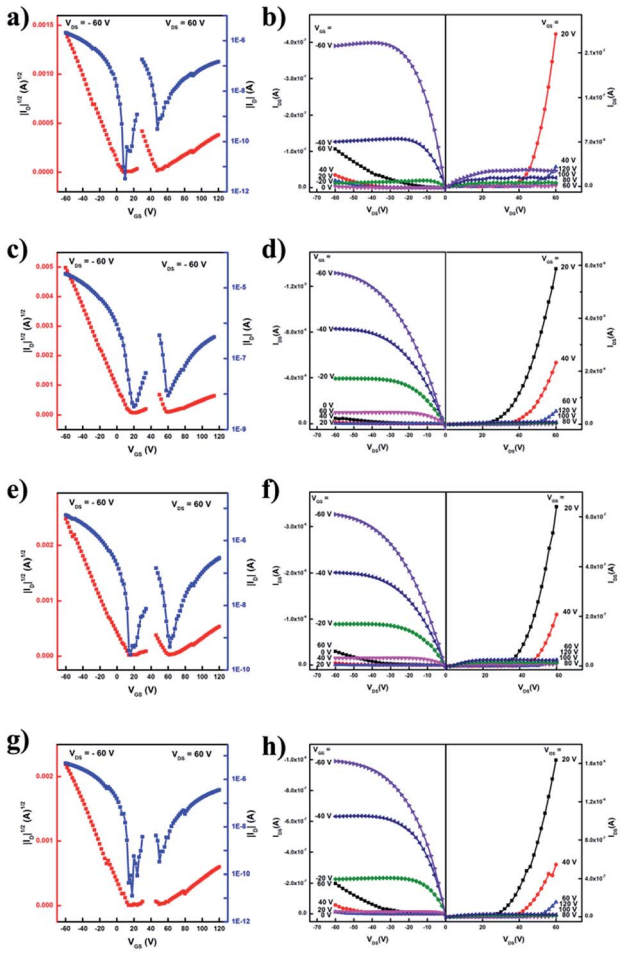

Fig. 3 Typical transfer (left) and output (right) curves of TGBC PFET devices based on (a and b) PTD-8-TVT; (c and d) PTD-10-TVT, (e and f) PTD-8-SVS, and (g and h) PTD-10-SVS thin films.

For the PFET devices, TGBC configurations can effectively reduce the negative influences from H_2O/O_2, which could enhance n-channel or ambipolar transport ability.[14] We fabricated TGBC PFET devices on silicon oxide in glovebox then measured in air. Fig. 3 shows the typical *I–V* characteristics of TGBC PFETs based on PTZDPP-based polymers and the device parameters are collected in Table 2. TZDPP-based polymers exhibit an ambipolar behaviour with an electron and hole mobilities reached up to 8.9×10^{-3} and 0.17 $cm^2\ V^{-1}\ s^{-1}$, respectively. Moreover, PFET device with bottom-gate bottom-contact (BGBC) configurations were also fabricated. The transfer and output curves are shown in Fig. S3† and the corresponding parameters are collected in Table S1 in the ESI.† The device geometry has a significant impact on the device performance of PFETs. The BGBC PFET devices exhibit only p-type behavior and no ambipolar behaviour behavior were detected. The length of the alkyl chains substituted on the TZDPP moieties has a profound influence on the FET performance of the corresponding polymers with the identical polymer backbone, which may arise from different lengths of branched side chains.[15] Interestingly, though PTD–SVS show a stronger aggregation tendency, the mobilities are much lower than those of the corresponding TVT-based polymers, which conflict with previous experimental observations. Some reports comparing the performance of polymers with different chalcogenophenes showed that the strong interchain Se interactions could readily improve mobilities.[16] The higher PDI values for SVS-based polymers may be one reason resulting in low mobility. Broader PDI indicates low molecular weight polymer chains or oligomers, which may act as traps for charge carrier, thus effecting charge transport in the FET devices.[8g] We then further resorted to other characterisations to explain this phenomenon as discussed below.

AFM was used to investigate surface morphology of the polymers for explaining this trend. Fig. 4 shows the typical AFM topographical images of the polymer thin films before and after annealing. The polymer films exhibit relatively homogeneous surface morphologies with the root-mean-square roughness (R_{RMS}) of 0.69–1.1 nm. Highly uniform intertwined polymer fibres and largely interconnected grains were observed from the AFM topographical images, which facilitate charge transport in the thin films and can be observed in reported high performance polymer semiconductors.[17] No clear change was observed in the annealed films compared to the as-cast ones. The presence of larger grains in the films of SVS-containing polymers compared with those of TVT-based polymers indicate the strong interchain interaction induced by the atom of selenium. However, large grains may not always be favour for obtaining higher mobility. The SVS-based polymer films have more defined gain boundaries, while TVT-based polymer films exhibit better connected ones, forming more uniform films.

Table 2 The properties of PFET devices with TGBC configurations and relevant crystallographic parameters of the polymers

	p-Channel			n-Channel				
	μ ($cm^2\ V^{-1}\ s^{-1}$)			μ ($cm^2\ V^{-1}\ s^{-1}$)				
Polymer	Average	Max	I_{on}/I_{off}	Average	Max	I_{on}/I_{off}	π–π spacing[a] (Å)	Lamellar spacing[a] (Å)
PTD-8-TVT	0.023	0.029	10^3 to 10^4	9.7×10^{-4}	1.1×10^{-3}	10^2 to 10^3	3.59	19.57
PTD-10-TVT	0.15	0.17	10^3 to 10^4	9.1×10^{-3}	9.7×10^{-3}	10^1 to 10^3	3.62	22.40
PTD-8-SVS	0.017	0.023	10^4 to 10^5	1.8×10^{-3}	2.4×10^{-3}	10^3 to 10^4	3.62	19.01
PTD-10-SVS	0.025	0.031	10^4 to 10^5	2.4×10^{-3}	3.8×10^{-3}	10^2 to 10^3	3.66	21.37

[a] The stacking distances calculated from the annealed films.

 This journal is © The Royal Society of Chemistry 2016

Published on 11 August 2016. Downloaded by Synchrotron Radiation Library on 11/09/2017 09:57:49.

To further investigate the relationship between carrier mobility and device performance, film crystallinity and microstructures were studied by 2D grazing-incidence X-ray diffraction (GIXRD). Fig. 5 displays the 2D-GIXRD patterns for the four polymers and the calculated stacking parameters are collected in Table 2. Clear diffraction peaks of (h00)s can be seen in the out-of-plane direction and an obvious (010) diffraction peak appears in the in-plane direction. The diffraction peaks reveal that all the polymers form a layer-by-layer lamellar packing with an edge-on orientation on the substrate, even in the absence of thermal annealing. This kind of stacking microstructure is beneficial for intrachain charge transport and was observed in high-performance polymers. The close lamellar π–π stacking distances were calculated to be around 3.6 Å for all the

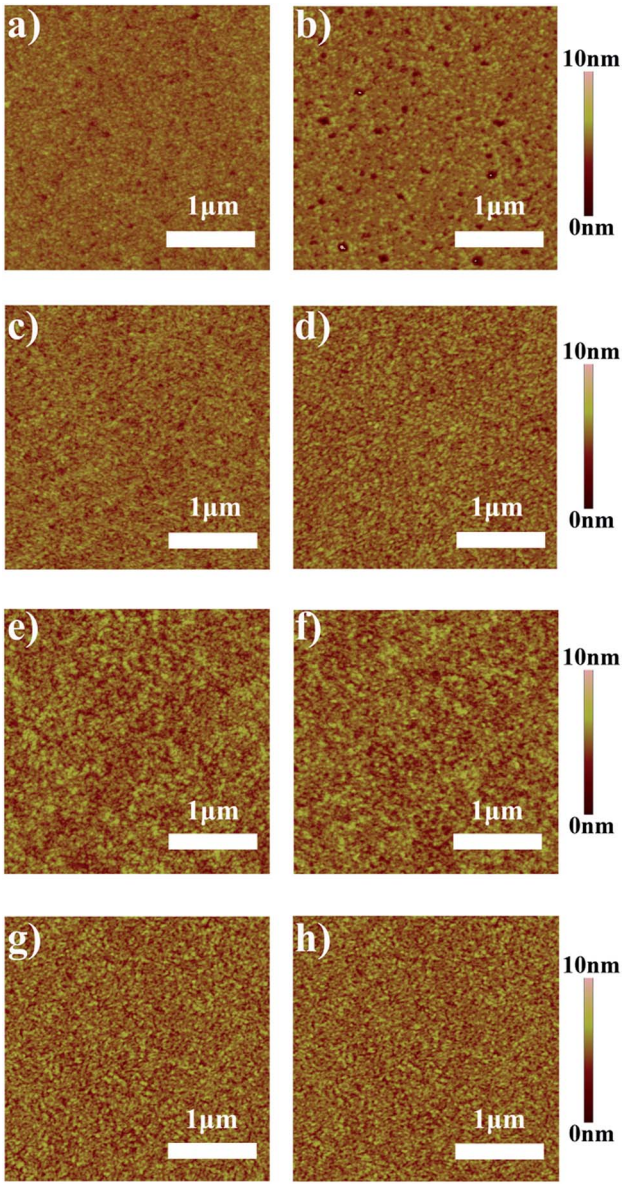

Fig. 4 AFM height images of (a and b) PTD-8-TVT, (c and d) PTD-10-TVT; (e and f) PTD-8-SVS, and (g and h) PTD-10-SVS thin films before (left) and after (right) annealing treatment.

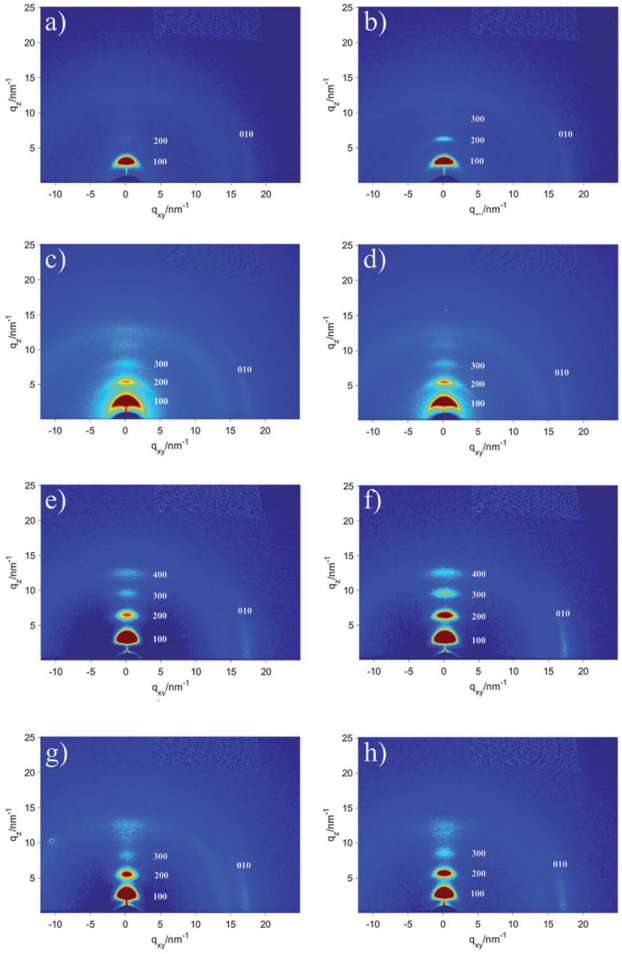

Fig. 5 GIXRD detector images of (a and b) PTD-8-TVT, (c and d) PTD-10-TVT, (e and f) PTD-8-SVS, and (g and h) PTD-10-SVS thin films before (left) and after (right) annealing treatment.

polymers, which arise from the strong interchain interactions induced by the strong electron-deficient nature of TZDPP. This provides an effective channel for interchain charge transport. Note that the TVT-based polymers reveal a small fraction of "face-on" textures, while for the SVS-containing polymers, the "edge-on" orientation is predominant. The "edge-on" textures with good alignment along the h00 planes with respect to the substrate generally facilitate interchain charge transport.[18] In addition, the stronger intensity of diffraction peaks indicate stronger crystallinity of the SVS-based polymers, which may be attributed to the stronger intermolecular interactions by replacing sulphur atoms with selenium atoms.[7,19] However, increase in mobility was not observed for the selenophene-containing polymers, and the polymers with longer side chains even show lower mobility by an order of magnitude.

Mean crystallite size and paracrystalline distortion parameter were calculated for further investigation into the films (Table 3). The mean crystallite size in the films is derived from the correlation length of (100) diffraction peak, which can be estimated using Scherrer equation. The (100) coherent domain sizes in the out-of-plane direction increased obviously after annealing treatment, suggesting decreased stacking defects and

Published on 11 August 2016. Downloaded by Synchrotron Radiation Library on 11/09/2017 09:57:49.

Table 3 Crystallographic information of the thin films

Polymer		Paracrystalline distortion parameter g (%)	FWHM (100) (°)	Correlation length (Å)
PTD-8-TVT	As-cast	18.49	0.883	14.32
	Anneal	12.23	0.504	25.10
PTD-10-TVT	As-cast	17.72	0.568	22.27
	Anneal	16.70	0.452	27.98
PTD-8-SVS	As-cast	17.79	0.736	17.19
	Anneal	15.63	0.535	23.65
PTD-10-SVS	As-cast	22.68	0.643	19.67
	Anneal	17.77	0.446	28.36

increased mean crystalline sizes. Though SVS-based polymers show stronger crystallinity, the increase in mean crystalline size was not so obvious. The paracrystallinity of the films can also be obtained from the GIXRD. Structural disorder in the paracrystalline films can be ascribed as random fluctuations in the lattice spacings.[20] The disorder was measured with paracrystalline distortion parameter (g), which is defined as the standard deviation of the local static lattice fluctuations normalized by the average value of the lattice spacing.[20,21] It can be calculated from the slope ($=g^2\pi^2/d$; d is the domain spacing) of the $\delta b - h^2$ plot, where h is the order of the diffractions and δb is the integral breadth of the corresponding diffraction peaks (Fig. S4†). Thermal annealing treatment could readily reduce the paracrystalline distortion parameter values, indicating more ordered films. In addition, for the polymers with the same side chain, though the molecules are more "edge-on" stacked, the values of SVS-based polymers exceeded those of TVT-based polymers, suggesting the films of selenophene containing polymers to be less ordered. The decreased mobility for the SVS-based polymers may arise from the less ordered and uniform films induced by the strong tendency to aggregate. By replacing sulphur atoms with selenium atoms, the enhanced intramolecular interactions decrease the solubility of the materials and aggregation among the precursors is induced in the solution, which lead to less uniform films. Recent studies also revealed the important role of solubility plays in enhancing device performance, and even beneficial influence through enhanced molecular contacts can even be countered by the reduced solubility.[22] Moreover, the mobility seems to be less determined by the molecular orientation.

Conclusions

Four TZDPP-based alternating D–A polymers were synthesized. The intramolecular oxygen–sulphur interaction promotes strong coplanarity and extended conjugation of the corresponding polymer backbone. Incorporation of the strong electron deficient moiety of TZDPP affords low-lying frontier orbital energy levels and close π–π stacking. Typical ambipolar charge carrier transport behaviour was achieved in TGBC devices. PTD-10-TVT exhibits the best performance with hole and electron mobilities of 0.17 and 9.7×10^{-3} cm^2 V^{-1} s^{-1}, respectively. Analyses of the films implied that though SVS-based polymers showed stronger crystallinity, the films are less ordered and uniform. This result suggests that a balance should be struck between the solubility and the interchain interactions to improve FET performance.

Acknowledgements

This work was financially supported by the Strategic Priority Research Program of the Chinese Academy of Sciences (XDB12030100) and the National Natural Science Foundation of China (21474116 and 51233006). The GIXRD results were tested at BL14B1 (Shanghai Synchrotron Radiation Facility), 23A1 Station (National Synchrotron Radiation Research Center, Taiwan), and 1W1A Station of Beijing Synchrotron Radiation Facility. The authors gratefully appreciate the assistance of scientists in the stations during the experiments.

Notes and references

1 (*a*) H. Yan, Z. Chen, Y. Zheng, C. Newman, J. R. Quinn, F. Dötz, M. Kastler and A. Facchetti, *Nature*, 2009, **457**, 679; (*b*) H. Sirringhaus, N. Tessler and R. H. Friend, *Science*, 1998, **280**, 1741; (*c*) Y. Li, *Acc. Chem. Res.*, 2012, **5**, 723; (*d*) W. Wu, Y. Liu and D. Zhu, *Chem. Soc. Rev.*, 2010, **39**, 1489; (*e*) C. Wang, H. Dong, W. Hu, Y. Liu and D. Zhu, *Chem. Rev.*, 2012, **39**, 2208.

2 (*a*) H. Chen, Y. Guo, G. Yu, Y. Zhao, J. Zhang, D. Gao, H. Liu and Y. Liu, *Adv. Mater.*, 2012, **24**, 4618; (*b*) J. Li, Y. Zhao, H. S. Tan, Y. L. Guo, C. A. Di, G. Yu, Y. Q. Liu, M. Lin, S. H. Lim, Y. Zhou, H. Su and B. S. Ong, *Sci. Rep.*, 2012, **2**, 754; (*c*) I. Kang, H. J. Yun, D. S. Chung, S. K. Kwon and Y. H. Kim, *J. Am. Chem. Soc.*, 2013, **135**, 14896; (*d*) H. R. Tseng, H. Phan, C. Luo, M. Wang, L. A. Perez, S. N. Patel, L. Ying, E. J. Kramer, T. Q. Nguyen, G. C. Bazan and A. J. Heeger, *Adv. Mater.*, 2014, **26**, 2993; (*e*) T. Lei, X. Xia, J.-Y. Wang, C.-J. Liu and J. Pei, *J. Am. Chem. Soc.*, 2014, **136**, 2135; (*f*) B. Sun, W. Hong, Z. Yan, H. Aziz and Y. Li, *Adv. Mater.*, 2014, **26**, 2636; (*g*) G. Kim, S.-J. Kang, G. K. Dutta, Y.-K. Han, T. J. Shin, Y.-Y. Noh and C. Yang, *J. Am. Chem. Soc.*, 2014, **136**, 9477; (*h*) Z. Cai, H. Luo, P. Qi, J. Wang, G. Zhang, Z. Liu and D. Zhang, *Macromolecules*, 2014, **47**, 2899; (*i*) J. Yao, C. Yu, Z. Liu, H. Luo, Y. Yang, G. Zhang and D. Zhang, *J. Am. Chem. Soc.*, 2016, **138**, 173; (*j*) Y. Ji, C. Xiao, Q. Wang, J. Zhang, C. Li, Y. Wu, Z. Wei, X. Zhan, W. Hu, Z. Wang, R. A. J. Janssen and W. Li, *Adv. Mater.*, 2016, **28**, 943.

3 (*a*) Z. Chen, M. J. Lee, R. Shahid Ashraf, Y. Gu, S. Albert-Seifried, M. M. Nielsen, B. Schroeder, T. D. Anthopoulos, M. Heeney, I. McCulloch and H. Sirringhaus, *Adv. Mater.*, 2012, **24**, 647; (*b*) H. Bronstein, Z. Chen, R. S. Ashraf, W. Zhang, J. Du, J. R. Durrant, P. S. Tuladhar, K. Song, S. E. Watkins, Y. Geerts, M. M. Wienk, R. A. J. Janssen, T. Anthopoulos, H. Sirringhaus, M. Heeney and I. McCulloch, *J. Am. Chem. Soc.*, 2011, **133**, 3272; (*c*) T. Lei, Y. Cao, Y. L. Fan, C. J. Liu, S. C. Yuan and J. Pei, *J. Am. Chem. Soc.*, 2011, **133**, 6099.

 This journal is © The Royal Society of Chemistry 2016

Published on 11 August 2016. Downloaded by Synchrotron Radiation Library on 11/09/2017 09:57:49.

4 (*a*) J. Letizia, M. Salata, C. Tribout, A. Facchetti, M. Ratner and T. Marks, *J. Am. Chem. Soc.*, 2008, **130**, 9679; (*b*) F. Kim, X. Guo, M. Watson and S. Jenekhe, *Adv. Mater.*, 2010, **22**, 478; (*c*) M. L. Zhu, H. Luo, L. P. Wang, G. Yu and Y. Q. Liu, *Acta Chim. Sin.*, 2012, **70**, 1599.

5 (*a*) J. D. Yuen, J. Fan, J. Seifter, B. Lim, R. Hufschmid, A. J. Heeger and F. Wudl, *J. Am. Chem. Soc.*, 2011, **133**, 20799; (*b*) I. McCulloch, R. S. Ashraf, L. Biniek, H. Bronstein, C. Combe, J. E. Donaghey, D. I. James, C. B. Nielsen, B. C. Schroeder and W. Zhang, *Acc. Chem. Res.*, 2012, **45**, 714; (*c*) J. F. Jheng, Y. Y. Lai, J. S. Wu, Y. H. Chao, C. L. Wang and C. S. Hsu, *Adv. Mater.*, 2013, **25**, 2445.

6 (*a*) B. Carsten, J. M. Szarko, L. Lu, H. J. Son, F. He, Y. Y. Botros, L. X. Chen and L. Yu, *Macromolecules*, 2012, **45**, 6390; (*b*) W. Li, W. S. C. Roelofs, M. Turbiez, M. M. Wienk and R. A. J. Janssen, *Adv. Mater.*, 2014, **26**, 3304; (*c*) C. Xiao, G. Zhao, A. Zhang, W. Jiang, R. A. J. Janssen, W. Li, W. Hu and Z. Wang, *Adv. Mater.*, 2015, **27**, 4963; (*d*) I. Bulut, P. Chávez, A. Mirloup, Q. Huaulmé, A. Hébraud, B. Heinrich, S. Fall, S. Méry, R. Ziessel, T. Heiser, P. Lévêque and N. Leclerc, *J. Mater. Chem. C*, 2016, **4**, 4296; (*e*) A. Zhang, Q. Wang, R. A. A. Bovee, C. Li, J. Zhang, Y. Zhou, Z. Wei, Y. Li, R. A. J. Janssen, Z. Wang and W. Li, *J. Mater. Chem. A*, 2016, **4**, 7736.

7 (*a*) I. Kang, T. K. An, J. Hong, H. J. Yun, R. Kim, D. S. Chung, C. E. Park, Y. H. Kim and S. K. Kwon, *Adv. Mater.*, 2013, **25**, 524; (*b*) H. Chen, Y. Guo, Z. Mao, G. Yu, J. Huang, Y. Zhao and Y. Liu, *Chem. Mater.*, 2013, **25**, 3589; (*c*) B. Kang, R. Kim, S. B. Lee, S.-K. Kwon, Y.-H. Kim and K. Cho, *J. Am. Chem. Soc.*, 2016, **138**, 3679.

8 (*a*) L. H. Jimison, M. F. Toney, I. McCulloch, M. Heeney and A. Salleo, *Adv. Mater.*, 2009, **21**, 1568; (*b*) H. N. Tsao, D. M. Cho, I. Park, M. R. Hansen, A. Mavrinskiy, D. Y. Yoon, R. Graf, W. Pisula, H. W. Spiess and K. Müllen, *J. Am. Chem. Soc.*, 2011, **133**, 2605; (*c*) L. Fang, Y. Zhou, Y.-X. Yao, Y. Diao, W.-Y. Lee, A. L. Appleton, R. Allen, J. Reinspach, S. C. B. Mannsfeld and Z. Bao, *Chem. Mater.*, 2013, **25**, 4874; (*d*) Z. Zhao, F. Zhang, Y. Hu, Z. Wang, B. Leng, X. Gao, C.-A. Di and D. Zhu, *ACS Macro Lett.*, 2014, **3**, 1174; (*e*) W. L. Leong, G. C. Welch, L. G. Kaake, C. J. Takacs, Y. Sun, G. C. Bazan and A. J. Heeger, *Chem. Sci.*, 2012, **3**, 2103; (*f*) W. R. Mateker, J. D. Douglas, C. Cabanetos, I. T. SachsQuintana, J. A. Bartelt, E. T. Hoke, A. E. Labban, P. M. Beaujuge, J. M. J. Frechet and M. D. McGehee, *Energy Environ. Sci.*, 2013, **6**, 2529; (*g*) H. D. Magurudeniya, R. S. Kularatne, E. A. Rainbolt, M. P. Bhatt, J. W. Murphy, E. E. Sheina, B. E. Gnade, M. C. Biewer and M. C. Stefan, *J. Mater. Chem. A*, 2014, **2**, 8773.

9 (*a*) T. Lei, J. H. Dou and J. Pei, *Adv. Mater.*, 2012, **24**, 6457; (*b*) F. C. Spano and C. Silva, *Annu. Rev. Phys. Chem.*, 2014, **65**, 477; (*c*) S. Shi, K. Shi, G. Yu, X. Li and H. Wang, *RSC Adv.*, 2015, **5**, 70319; (*d*) X. Liu, J. Huang, J. Xu, D. Gao, W. Zhang, K. Shi and G. Yu, *RSC Adv.*, 2016, **6**, 35394; (*e*) C.-J. Chaing, J.-C. Chen, Y.-J. Kuo, H.-Y. Tsao, K.-Y. Wub and C.-L. Wang, *RSC Adv.*, 2016, **6**, 8628.

10 (*a*) J. S. Lee, S. K. Son, S. Song, H. Kim, D. R. Lee, K. Kim, M. J. Ko, D. H. Choi, B. S. Kim and J. H. Cho, *Chem. Mater.*, 2012, **24**, 1316; (*b*) M. Kaur, D. S. Yang, J. Shin, T. W. Lee, K. Choi, M. J. Cho and D. H. Choi, *Chem. Commun.*, 2013, **49**, 5495; (*c*) M. Gruber, S.-H. Jung, S. Schott, D. Venkateshvaran, A. J. Kronemeijer, J. W. Andreasen, C. R. McNeill, W. W. H. Wong, M. Shahid, M. Heeney, J.-K. Lee and H. Sirringhaus, *Chem. Sci.*, 2015, **6**, 6949; (*d*) Z. Mao, W. Zhang, J. Huang, K. Shi, D. Gao, Z. Chen and G. Yu, *Polym. Chem.*, 2015, **6**, 6457; (*e*) A. Keerthi, C. An, M. Li, T. Marszalek, A. G. Ricciardulli, B. Radha, F. D. Alsewailem, K. Müllenand and M. Baumgarten, *Polym. Chem.*, 2016, **7**, 1545; (*f*) D. Gao, K. Tian, W. Zhang, J. Huang, Z. Chen, Z. Mao and G. Yu, *Polym. Chem.*, 2016, **7**, 4046; (*g*) K. Miao, G. J. Chae, X. Wu, Q. Shu, X. Zhu, B. Sun, J. Fan and S. Cho, *RSC Adv.*, 2016, **6**, 29164.

11 (*a*) A. J. Cohen, P. Mori-Sanchez and W. Yang, *Science*, 2008, **321**, 792; (*b*) A. J. Cohen, P. Mori-Sanchez and W. Yang, *Chem. Rev.*, 2011, **112**, 289; (*c*) N. E. Jackson, B. M. Savoie, K. L. Kohlstedt, M. O. Cruz, G. C. Schatz, L. X. Chen and M. A. Ratner, *J. Am. Chem. Soc.*, 2013, **135**, 10475.

12 (*a*) F. He, W. Wang, W. Chen, T. Xu, S. B. Darling, J. Strzalka, Y. Liu and L. Yu, *J. Am. Chem. Soc.*, 2011, **133**, 3284; (*b*) Z. Li, Y. Zang, C.-C. Chueh, N. Cho, J. Lu, X. Wang, J. Huang, C.-Z. Li, J. Yu and A. K.-Y. Jen, *Macromolecules*, 2014, **47**, 7407.

13 (*a*) I. Meager, M. Nikolka, B. C. Schroeder, C. B. Nielsen, M. Planells, H. Bronstein, J. W. Rumer, D. James, R. S. Ashraf, A. Sadhanala, P. Hayoz, J.-C. Flores, H. Sirringhaus and I. McCulloch, *Adv. Mater.*, 2014, **24**, 7109; (*b*) H. J. Yun, H. H. Choi, S. K. Kwon, Y. H. Kim and K. Cho, *Chem. Mater.*, 2014, **26**, 3928.

14 (*a*) H. Yan, Z. H. Chen, Y. Zheng, C. Newman, J. R. Quinn, F. Dötz, M. Kastler and A. Facchetti, *Nature*, 2009, **457**, 679; (*b*) L. Zhang, C. A. Di, Y. Zhao, Y. L. Guo, X. N. Sun, Y. G. Wen, W. Y. Zhou, X. W. Zhan, G. Yu and Y. Q. Liu, *Adv. Mater.*, 2010, **22**, 3537; (*c*) H. Chen, Y. Guo, Z. Mao, G. Yu, J. Huang, Y. Zhao and Y. Liu, *Chem. Mater.*, 2013, **25**, 3589.

15 (*a*) Y. Li, S. P. Singh and P. Sonar, *Adv. Mater.*, 2010, **22**, 4862; (*b*) S. Subramaniyan, H. Xin, F. S. Kim, S. Shoaee, J. R. Durrant and S. A. Jenekhe, *Adv. Energy Mater.*, 2011, **1**, 854; (*c*) J. Shin, G. E. Park, D. H. Lee, H. A. Um, T. W. Lee, M. J. Cho and D. H. Choi, *ACS Appl. Mater. Interfaces*, 2015, **7**, 3280.

16 (*a*) E. H. Jung, S. Bae, T. W. Yoo and W. H. Jo, *Polym. Chem.*, 2014, **5**, 6545; (*b*) R. S. Ashraf, I. Meager, M. Nikolka, M. Kirkus, M. Planells, B. C. Schroeder, S. Holliday, M. Hurhangee, C. B. Nielsen, H. Sirringhaus and I. McCulloch, *J. Am. Chem. Soc.*, 2015, **137**, 1314.

17 (*a*) J. H. Park, E. H. Jung, J. W. Jung and W. H. Jo, *Adv. Mater.*, 2013, **25**, 2583; (*b*) B. Sun, W. Hong, Z. Q. Yan, H. Aziz and Y. N. Li, *Adv. Mater.*, 2014, **26**, 2636; (*c*) H. J. Yun, J. Cho,

Published on 11 August 2016. Downloaded by Synchrotron Radiation Library on 11/09/2017 09:57:49.

D. S. Chung, Y. H. Kim and S. K. Kwon, *Macromolecules*, 2014, **47**, 7030.

18 (*a*) W. H. Lee, J. Park, S. H. Sim, S. Lim, K. S. Kim, B. H. Hong and K. Cho, *J. Am. Chem. Soc.*, 2011, **133**, 4447; (*b*) J. Shin, H. A. Um, D. H. Lee, T. W. Lee, M. J. Cho and D. H. Choi, *Polym. Chem.*, 2013, **4**, 5688; (*c*) M. Jang, J.-H. Kim, D. H. Hwang and H. Yang, *ACS Appl. Mater. Interfaces*, 2015, **7**, 12781.

19 (*a*) M. Shahid, R. S. Ashraf, Z. Huang, A. J. Kronemeijer, T. M. Ward, I. McCulloch, J. R. Durrant, H. Sirringhaus and M. Heeney, *J. Mater. Chem.*, 2012, **22**, 12817; (*b*) A. J. Kronemeijer, E. Gili, M. Shahid, J. Rivnay, A. Salle, M. Heeney and H. Sirringhaus, *Adv. Mater.*, 2012, **24**, 1558.

20 (*a*) D. Yoo, B. Nketia-Yawson, S.-J. Kang, H. Ahn, T. J. Shin, Y.-Y. Noh and C. Yang, *Adv. Funct. Mater.*, 2015, **25**, 586; (*b*) J. Y. Na, B. Kang, D. H. Sin, K. Cho and Y. D. Park, *Sci. Rep.*, 2015, **5**, 13288.

21 A. M. Hindeleh and R. Hosemann, *J. Phys. C: Solid State Phys.*, 1988, **21**, 4155.

22 M. Al-Hashimi, Y. Han, J. Smith, H. S. Bazzi, S. Y. A. Alqaradawi, S. E. Watkins, T. D. Anthopoulos and M. Heeney, *Chem. Sci.*, 2016, **7**, 1093.

This journal is © The Royal Society of Chemistry 2016